A method for the registration of spectral images of paintings and its evaluation

Zacharopoulos, Athanasios; Hatzigiannakis, Kostas; Karamaoynas, Polykarpos; Papadakis, Vassilis M.; Andrianakis, Michalis; Melessanaki, Kristalia; Zabulis, Xenophon

DOI
10.1016/j.culher.2017.07.004

Publication date
2018

Document Version
Final published version

Published in
Journal of Cultural Heritage

Citation (APA)
Zacharopoulos, A., Hatzigiannakis, K., Karamaoynas, P., Papadakis, V. M., Andrianakis, M., Melessanaki, K., & Zabulis, X. (2018). A method for the registration of spectral images of paintings and its evaluation. *Journal of Cultural Heritage*, *29*, 10-18. https://doi.org/10.1016/j.culher.2017.07.004

Journal of Cultural Heritage 29 (2018) 10–18

Available online at
ScienceDirect
www.sciencedirect.com

Elsevier Masson France
EM|consulte
www.em-consulte.com/en

Original article

A method for the registration of spectral images of paintings and its evaluation

Athanasios Zacharopoulos[a], Kostas Hatzigiannakis[a], Polykarpos Karamaoynas[b], Vassilis M. Papadakis[a,c], Michalis Andrianakis[a], Kristalia Melessanaki[a], Xenophon Zabulis[b,*]

[a] Institute for Electronic Structure and Laser, Foundation for Research and Technology-Hellas, N. Plastira 100, Heraklion 700 13, Greece
[b] Institute of Computer Science, Foundation for Research and Technology-Hellas, N. Plastira 100, Heraklion 700 13, Greece
[c] Aerospace Non-Destructive Testing Laboratory, Faculty of Aerospace Engineering, Delft University of Technology (Aerondt), Kluyverweg 1, 2600 GB Delft, The Netherlands

ARTICLE INFO

Article history:
Received 11 October 2016
Accepted 7 July 2017
Available online 4 August 2017

Keywords:
Spectral imaging
Spectral cube
Paintings
Spectroscopy
Image registration

ABSTRACT

This work concerns the automatic registration of spectral images of paintings upon planar, or approximately planar, surfaces. An approach that capitalizes upon this planarity is proposed, which estimates homography transforms that register the spectral images into an aligned spectral cube. Homography estimation methods are comparatively evaluated for this purpose. A non-linear, robust estimation method that is based on keypoint features is adopted, as the most accurate. A marker-based, quantitative evaluation method is proposed for the measurement of multispectral image registration accuracy and, in turn, utilized for the comparison of the proposed registration method to the state of the art. For the same purpose, characteristic for this application domain, benchmark datasets that are annotated with correctly corresponding points have been compiled and are publicly availed.

1. Introduction

Multispectral imaging (MSI) is a non-destructive diagnostic technique, combining digital imaging with spectroscopic analysis, to recover spatial and spectral information about a surface or an object. MSI is applied in medicine, agriculture, remote sensing, food industry, and cultural heritage sciences, including art conservation, archeology, and art history [1,2].

In MSI, a monochromator, i.e. a series of bandpass filters, is placed in front of the illumination system or the imaging sensor. This sensor then acquires a sequence of quasi-monochromatic images at consecutive narrow spectral bands, mainly in the visible spectrum but often extending to the infrared (IR) and/or the ultraviolet (UV). The acquired grayscale images are called *spectral images* and their sequence a *spectral cube*.

Analysis of the spectral cube provides information related to stratigraphy of a painting, that is the paint layers that comprise it. The intensity values along a column of the spectral cube form the extracted reflectance spectrum, at the column location. This spectrum is informative about the imaged materials and used in pigment studies [3–5]. Revealing the pigments used in artworks, assists the conservation process as well as studies in art history [2,6]. In some cases only traces of the material are present, casting the spatial accuracy of measurements crucial.

The filter wheel approach to MSI is widely used and allows portability [7,5]. As different wavelengths follow different optical paths inside optics [8], focus readjustments are needed between acquisition of spectral images. This refocusing changes focal length and the Field of View (FOV). In addition, portability implies low-weight instrumentation as well as flexible and modular supports, which are sensitive to vibrations. Both of these factors lead to misalignment between the acquired spectral images. Registration of these spectral images is required before spectrum extraction, so that a physical point is imaged at the same coordinates in all images of the spectral cube.

In the review paper [9], registration methods are respectively identified as local or global, depending on if the matched features are points or entire image areas. In the domain of cultural heritage, image registration has been employed in the alignment of spectral images for the creation of spectral cubes.

Concerning global MSI registration methods that have been used to create aligned spectral cubes, correlation based registration has

* Corresponding author.
E-mail address: zabulis@ics.forth.gr (X. Zabulis).

https://doi.org/10.1016/j.culher.2017.07.004
1296-2074/

been used in [10–12]. In [8,13], aberrations due to filters are compensated based on Mutual Information (MI), but registration errors due to vibrations are not considered. In [14], registration is based on the Fourier–Mellin transform.

Local MSI registration methods require point correspondences between the images to be registered. These correspondences are established by 1-1 matching of keypoint features, between image pairs. In [15,16], cross correlation of keypoint neighborhoods is used to find matches. In [17,18], the Scale Invariant Feature Transform (SIFT) features are utilized to find matches and spurious matches are reduced using the Random Sample Consensus (RANSAC) [19]. In [20,21], local features are utilized to register images in a piecemeal fashion, by tessellating images into patches. However, to avoid textureless patches, which are poor in keypoint features, tessellation is supervised [21].

Quantitative accuracy evaluation enables comparative assessment of registration methods. In the aforementioned works, evaluation is conducted qualitatively rather than quantitatively. An exception is [21], which utilizes a line grid for this purpose. However, line thickness introduces uncertainty. In addition, the grid is visible in a subset of the spectrum, thus hindering evaluation in some bands.

Contributions of this work are the following: (i) a local multispectral image registration method for planar surfaces that estimates homography transformations between images, (ii) a marker-based approach for the quantitative evaluation of multispectral registration methods, (iii) five publicly available benchmark datasets for the evaluation of registration accuracy of MSI of paintings that cover characteristic application scenarios, and (iv) a comparative experimental evaluation, of the proposed method against pertinent state of the art methods.

This work is motivated by the acquisition of spectral cubes from planar surfaces that belong to cultural heritage objects. Focus is placed upon the most dominant and representative type of such surfaces, which are paintings, e.g. panel paintings, easel paintings, or wall paintings. We believe that more types of planar surfaces such as, for instance, manuscripts, printed matter, textiles, or tapestries can also be treated in the same way. We, thus, warrant the continuation of pertinent experimental studies, in future work.

2. The proposed approach

2.1. Preliminaries

The proposed approach is illustrated in Fig. 1. A multispectral camera with a filter wheel images a planar surface. Imaging distance is assumed sufficiently large so that deviations of surface shape from planarity and penetration of wavelengths within the surface are both assumed negligible.

In an ideal setup, Fig. 1(a), the scene is imaged by a static camera and light travels the same optical path length through any of the interchangeable filters and camera lens. Consequently, impact is the same for all filters and switching between them would not affect focus. Images of a spectral sequence $I_i, i \in [1, N]$, are simply stacked to obtain an aligned spectral cube $\mathcal{S}$.

In practice, the optical path length is not the same for all wavelengths and switching between filters affects focus [8,14]. Focus is then readjusted, affecting FOV and, thus, image scaling. Refocusing and accidental vibrations between image acquisitions result in minute changes of camera pose. The combined effect of both factors results in a sequence of misaligned images Fig. 1(b). We assume an optical lens of narrow FOV and negligible lens distortion. We acknowledge that lens distortion compensation would improve results and plan this for future work.

A homography is a perspective transformation between two images of the same planar surface, which predicts the effects due to changes in camera pose and image scaling. Its number of Degrees of Freedom (DOF) is 8 and it is represented by a 3×3 matrix $\mathbf{H}$. A homogeneous 2D point upon the *transformed* image, $\mathbf{p} = [\, x \quad y \quad 1 \,]^T$, is *transferred* to the corresponding location $\mathbf{q}$ in the *reference* image as $\mathbf{q} = \mathbf{H} \cdot \mathbf{p}$, where $\cdot$ denotes matrix multiplication. Finding point correspondences between the two images, enables the estimation of homography $\mathbf{H}$ which warps the transformed image upon the reference, Fig. 1(c). The homography between images I_i and I_j is denoted as $\mathbf{H}_{i,j}$. Using the estimated transformations, all images are registered to a reference image in the sequence, yielding the aligned spectral cube $\mathcal{S}$, Fig. 1(d).

MSI practice requires the camera axis to be oriented perpendicularly to the imaged painting. It ought to be noted that homography estimation and, hence, the proposed approach, do

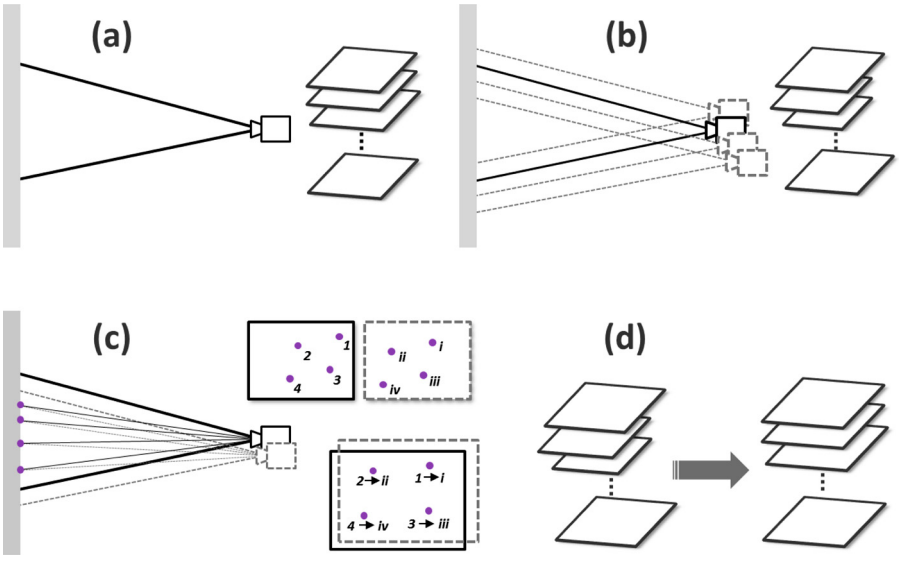

Fig. 1. Method overview. Geometry of (a) ideal and (b) realistic spectral cube acquisition; (c) feature point matches between two spectral images are used to estimate the homography transformation that registers them; (d) sequential registration of all images provides an aligned spectral cube.

not assume a perpendicular configuration and can be applied to a broader range of orientations. In the context of this work, mild deviations from the perpendicular configuration are treated without any modification or tuning of the registration method.

2.2. MSI registration

In overview, the registration method is as follows. Initially, keypoint features in consecutive images of the spectral sequence are detected and matched. Using these matches, the homography transformations for consecutive images are robustly estimated. By sequentially linking these estimates, the spectral images are registered to a reference image in the sequence, resulting in an aligned spectral cube.

More specifically, SIFT features are detected in images I_i, at locations $\mathbf{q}_{i,k}$. The detected keypoints are matched, as in [22]. For robustness, matches are required to be symmetric [23]. All available bits of pixel depth are utilized. For our experiments, library [24] was modified to treat also 16-bit images (see Section 3.1). In preliminary experiments, it was confirmed that the entire dynamic range increases matching robustness. This is attributed to the better keypoint descriptions obtained due to the additional information.

Two arbitrary images from the spectral sequence may be quite different for feature matching to be fruitful. Images acquired at adjacent spectral bands are more similar and, hence, correspondences are searched in consecutive images. Homography $\mathbf{H}_{i,i+1}$, for consecutive images I_i and I_{i+1} is estimated using the *homest* method [25], which robustly copes with spurious correspondences. Point coordinates are normalized to improve conditioning [26]. Least Median of Squares linear fit is applied to reject spurious matches [27]. Non-linear refinement of the linear homography estimate is performed by minimization of the transfer error, using the Levenberg–Marquardt algorithm [28], as implemented in [29]. This error is symmetric, thus ordering of the image pair is not of concern.

Let I_v be the reference image. Choosing I_v in the middle of the spectrum (i.e. instead of the beginning) reduces the accumulation of error due to the sequential linking of homography transforms. Furthermore, images at the extremes of the spectrum are relatively more sensitive to noise and contain less features. Homographies $\mathbf{H}_{v,i}$ are computed as:

$$\mathbf{H}_{v,i} = \begin{cases} \mathbf{H}_{v,v-1} \cdot \mathbf{H}_{v-1,v-2} \ldots \mathbf{H}_{i+2,i+1} \cdot \mathbf{H}_{i+1,i} & \text{if } i < v \\ \mathbf{H}_{v,v+1} \cdot \mathbf{H}_{v+1,v+2} \ldots \mathbf{H}_{i-2,i-1} \cdot \mathbf{H}_{i-1,i} & \text{if } i > v \\ \mathbf{I}_{3\times 3} & \text{if } i = v, \end{cases} \quad (1)$$

where $\mathbf{H}_{i+1,i} = \mathbf{H}_{i,i+1}^{-1}$, and $\mathbf{I}_{3\times 3}$ the 3×3 identity matrix. Besides projective (8 DOF), the work in [25] estimates also affine homographies (6 DOF); these two variants are referred to as *homest8* and *homest6*, respectively.

Finally, images I_i are resampled, or "warped", using the estimated homographies and bilinear interpolation. Image S_i is computed, warping image I_i according to $\mathbf{H}_{v,i}$. Stacking images S_i comprises $\mathcal{S}$.

2.3. Accuracy evaluation

To quantitatively evaluate registration accuracy, correct point correspondences across all images are utilized. These correspondences are due to the matching of physical landmarks across all spectral images. The correspondences established between the matched landmarks, as well as, the associated image point locations of these landmarks are henceforth called *ground truth*.

As landmarks are static upon the imaged surface, they should be coincident in accurately registered images. Registration error for a pair (I_v, I_i), is the mean distance between landmark points in the transformed image and their corresponding points in I_v.

Let μ be the number and $\mathbf{u}_{v,k}, (k = 1, \ldots, \mu)$ the locations of landmark points in I_v. Let $\mathbf{u}_{i,k}$ be the locations of landmarks in any I_i of the remaining images. The locations of the transformed landmarks from I_i to I_v, are $\mathbf{q}_{i,k} = \mathbf{H}_{v,i} \cdot \mathbf{u}_{i,k}$. Registration error of a sequence is the mean error between all registered spectral image pairs:

$$E = \frac{\sum_{i=1, i\neq v}^{N} \sum_{k=1}^{\mu} \|\mathbf{u}_{v,k} - \mathbf{q}_{i,k}\|}{(N-1)\cdot\mu}. \quad (2)$$

The *original error* before registration, that is creating $\mathcal{S}$ by stacking original images I_i, is denoted E_0 and computed by substituting $\mathbf{q}_{i,k}$ with $\mathbf{u}_{i,k}$ in Eq. (2).

Albeit images are matched sequentially, error is measured according to I_v. This way, residual errors that are propagated through registrations are accounted and the effective error of the end result is measured.

3. Experiments

The employed MSI apparatus is presented in Section 3.1, followed by a qualitative and computational evaluation of our implementation (Section 3.2). To perform the quantitative evaluation, datasets annotated with ground truth were compiled (Section 3.3). Using these datasets, variants of the proposed method are evaluated comparatively and against state of the art (Section 3.4). The aforementioned datasets are publicly availed,[1] along with a technical report on their collection [30].

3.1. Image acquisition and preprocessing

The experiments were conducted with the IRIS II, a portable MSI system mainly comprised of a CMOS camera and a filter wheel. In the experiments, $N = 23$ filters were utilized ranging from UV (350–400 nm, BP10nm), to visible (400–700 nm, BP25nm), and to near IR (700–1200 nm, BP25nm). Dynamic range is 8 bits and resolution is 2560×2048 pixels. A 25 mm, f/1.3 lens was used. The camera optical axis was adjusted perpendicularly to the artwork surface. Illumination comprised of two tungsten halogen lamps for the visible and NIR bands and two black light fluorescent lamps for the UV band; all posed, $\approx 45^\circ$ to the object surface.

For each spectral band i, henceforth called "wavelength", a standard acquisition process is followed. Originally, focus is adjusted. Following, a white, highly reflective target (Spectralon, $R \approx 99\%$ @350–1200 nm, Labsphere) is placed in front of the object. The upper level of the camera dynamic range is adjusted to reach the maximum possible mean intensity, without saturation. "White" image, W, is acquired. The white target is removed and, keeping all settings unchanged, the acquisition of spectral image Q follows. Still keeping settings unchanged, light entrance is blocked in front of the camera and a "Black" image, B, is captured, corresponding to the dark current of the camera.

Intensity normalization is performed independently for each spectral image and for each pixel $\mathbf{x}$, to produce I_i as:

$$I_i(\mathbf{x}) = \frac{Q_i(\mathbf{x}) - B_i(\mathbf{x})}{W_i(\mathbf{x}) - B_i(\mathbf{x})}, \quad (3)$$

The quotient is in [0, 1] and correlated to the reflectance of the studied area.

[1] At http://www.ics.forth.gr/cvrl/msi.

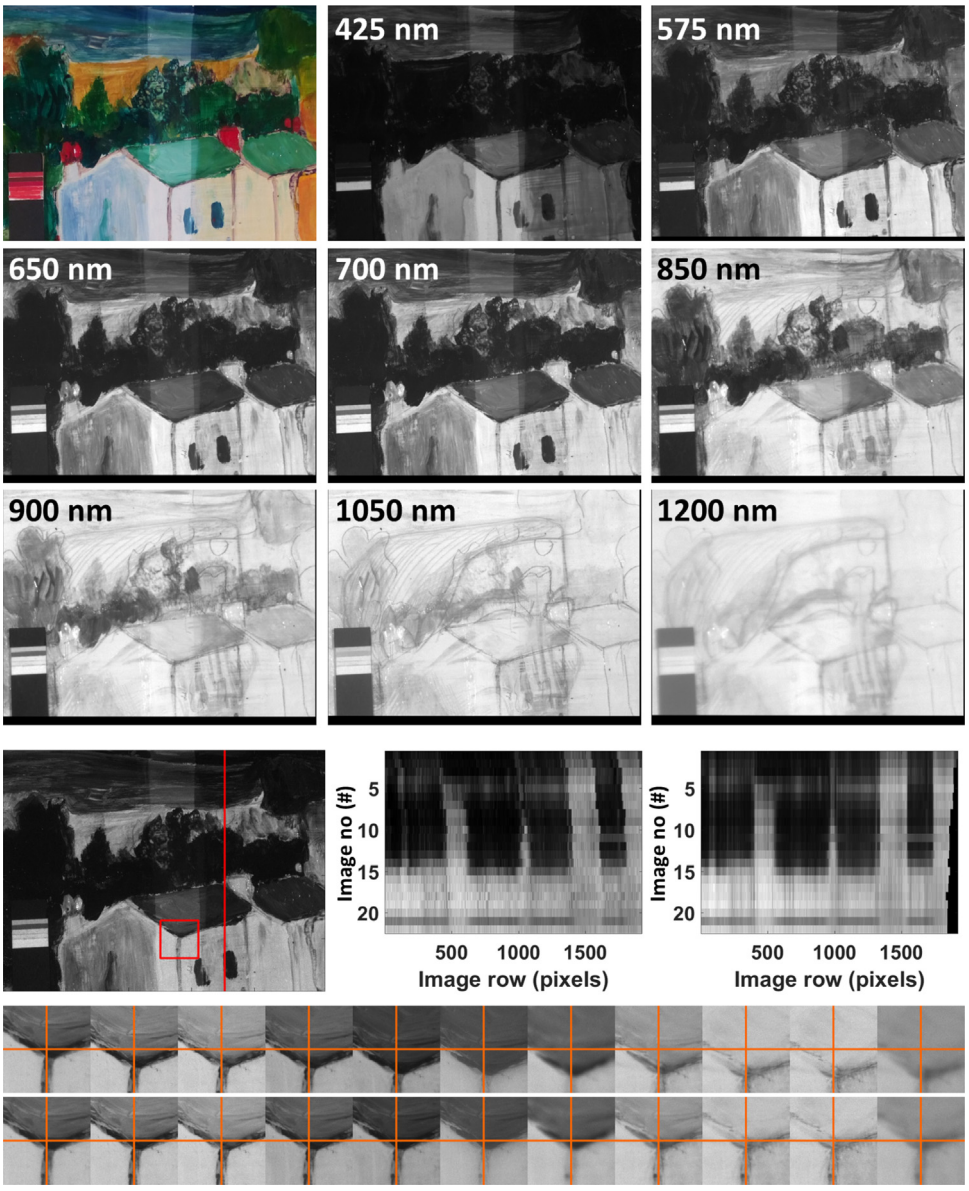

Fig. 2. Qualitative evaluation. Top 3 rows: color image of the target and registration results using the homest method for 8 out of the 23 spectral images of a sequence. Middle: marked reference image and slices of $\mathcal{S}$ before (center) and after (right) registration, along the marked line. Last 2 rows: I_i and S_i in the marked 301×301 pixel region, respectively, for indicative spectral cube layers, between 425 and 1150 nm. A cross-hair overlay upon each, facilitates comparative inspection. (For interpretation of the references to color in text, the reader is referred to the web version of the article.)

3.2. Qualitative evaluation and computational cost

For a qualitative evaluation, a multispectral sequence from a painting without markers was acquired. In Fig. 2, the results are overviewed. A detailed assessment of accuracy is presented, in the last two rows. An image column and a square image region are marked in red, upon the reference image. The contents of $\mathcal{S}$ for the marked column and region are shown, before and after registration.

Implementation was in C/C++ and accompanied with a Graphical User Interface, facilitating input selection and visualization of results. During the processing of 23, 2560×1920 images, 229,017 features were detected and 77,812 correspondences were established, estimating 22 homographies. Feature detection and matching was parallelized using OpenMP [31] and executed in 281 s on an 8-core CPU at 3.07 GHz with 6 GB of RAM (see [30], for more details).

3.3. Datasets and ground truth annotation

To quantitatively assess accuracy, MSI sequences annotated with ground truth are required. To the best of our knowledge, such datasets are not publicly available. Thus, we created five such datasets using paintings and configurations that cover characteristic application scenarios. Visual features of painted surfaces are wavelength dependent and manual annotation is prone to error. Thus, μ markers visible in all I_i were utilized.

Small markers were printed using the design of a 2×2 checkerboard, clearly distinguishable in each wavelength. Marker size was adjusted depending on imaging distance, so that markers would appear in $\approx 40 \times 40$ pixels in I_i. Markers were arranged in a 4×4 grid. Evaluation artifacts are shown in Fig. 3.

Landmarks were the inner checkerboard corners. They were localized in images as in [32]. Correspondences were established

Fig. 3. Evaluation artifacts. Left: color image of the mock-up painting, with landmarks. Middle: color image of the Byzantine icon, with landmarks. Right: the design used to print landmarks (top) and close-up on an imaged landmark (bottom).

Table 1
Mean average (and std) of original and registration errors, in pixels, using the five datasets in Section 3.3.

Dataset	D1	D2	D3	D4	D5
E_0	11.22 (5.08)	9.57 (6.34)	17.43 (15.13)	11.71 (4.75)	19.26 (11.48)
homest6	0.67 (0.11)	0.69 (0.13)	0.77 (0.09)	0.78 (0.35)	0.64 (0.14)
homest8	1.15 (0.72)	0.98 (0.53)	0.95 (0.27)	0.96 (0.49)	0.84 (0.31)
RANSAC	1.29 (0.55)	0.92 (0.35)	1.27 (0.60)	2.17 (2.22)	1.49 (0.87)
LMedS	0.99 (0.38)	0.76 (0.23)	0.94 (0.23)	1.07 (0.58)	0.92 (0.43)
SAD	4.73 (3.19)	6.11 (4.81)	3.98 (3.04)	3.19 (1.92)	3.26 (1.91)
MI	6.80 (4.71)	NA	4.77 (3.22)	4.22 (3.64)	3.21 (1.87)
NCC	5.60 (3.46)	6.06 (4.84)	4.34 (2.52)	3.34 (2.32)	3.36 (2.34)
FM	3.84 (2.99)	7.08 (6.95)	3.43 (2.57)	3.40 (1.71)	3.03 (1.97)

Table 2
Mean average (and std) of original and registration errors, in mm, for the five datasets, in Section 3.3.

Dataset	D1	D2	D3	D4	D5
E_0	0.83 (0.37)	0.97 (0.64)	1.77 (1.54)	1.19 (0.48)	1.96 (1.16)
homest6	0.05 (0.00)	0.07 (0.01)	0.07 (0.00)	0.08 (0.03)	0.06 (0.01)
homest8	0.09 (0.05)	0.07 (0.04)	0.07 (0.02)	0.10 (0.05)	0.09 (0.03)
RANSAC	0.09 (0.04)	0.09 (0.03)	0.13 (0.06)	0.22 (0.22)	0.15 (0.08)
LMedS	0.07 (0.02)	0.07 (0.02)	0.09 (0.02)	0.10 (0.06)	0.09 (0.04)
SAD	0.35 (0.23)	0.62 (0.49)	0.40 (0.31)	0.32 (0.19)	0.33 (0.19)
MI	0.50 (0.35)	NA	0.48 (0.32)	0.43 (0.37)	0.32 (0.19)
NCC	0.41 (0.25)	0.61 (0.49)	0.44 (0.25)	0.34 (0.23)	0.34 (0.23)
FM	0.28 (0.22)	0.72 (0.70)	0.34 (0.26)	0.34 (0.17)	0.30 (0.20)

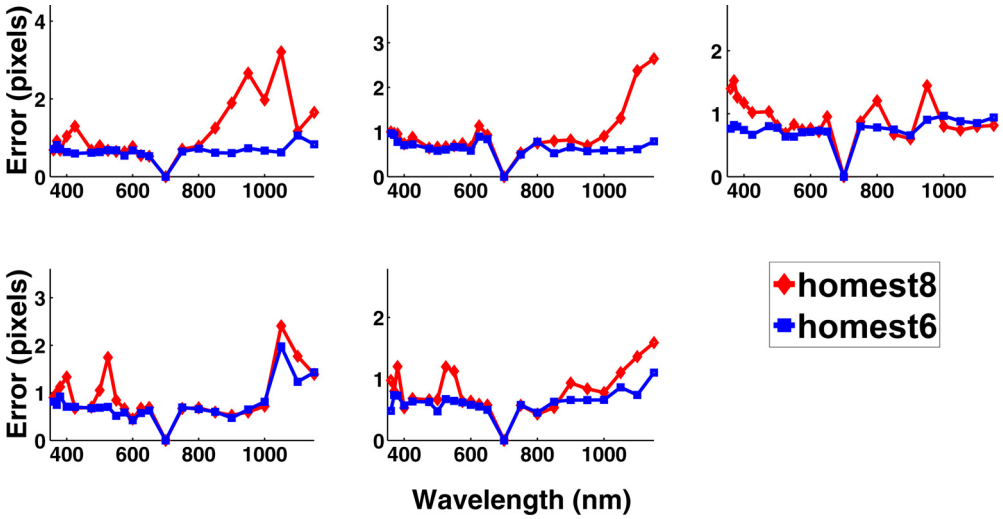

Fig. 4. Registration errors for affine (homest6) and projective (homest8) homography estimation, as a function of wavelength, for D1–D5 (left to right, top to bottom).

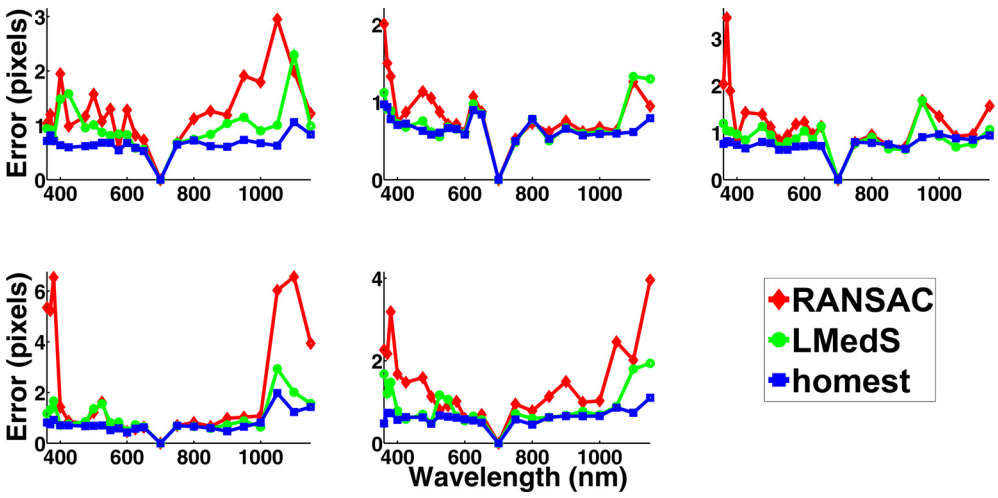

Fig. 5. Registration errors for homest, RANSAC and LMedS as a function of wavelength, for D1–D5 (left to right, top to bottom).

between image locations where the same landmark appears. These corresponding image locations, $\mathbf{u}_{i,k}$, comprise the ground truth annotation of the dataset. The following datasets were collected, each containing 23 images and ground truth annotation:

D1. To simulate typical artworks, a mock-up painting was created upon a wooden panel coated with white tempera. A cubist sketch of a woman's head was drawn with pencil. Over it, a draft drawing of a landscape with two houses was painted using a variety of temperas, fully covering the pencil drawings. To finish, two varnish layers were applied, a dammar varnish on the left and a mastic varnish on the right side, leaving a vertical band in the middle with no vanish, as a color dependent reference area. Imaging distance was ≈86.5 cm. FOV covered 190 mm by 142 mm. Marker size was 25 mm^2.

D2. A Byzantine icon was used, painted in egg tempera with gold leaf, on a planar wooden surface. It portrays "Saint John the Baptist", in a green mantle and blue fore tunic against a gold background, Fig. 3. Imaging distance was ≈86.5 cm. FOV covered 190 × 142 mm^2. Marker size was 25 mm^2.

D3. The setup of D1 was replicated by attaching the camera to a tripod, to simulate real cases of on-site acquisition.

D4. In the setup of D3, imaging distance was increased to ≈120 cm. FOV covered 267 × 200 mm^2. Marker size was 34.6 mm^2.

D5. Using the setup and markers of D4, a small deviation 3.75° angle was introduced to the perpendicularity between the camera and the painting. It simulates a typical error in the, ideally perpendicular, camera placement, in cases of on-site image acquisition.

3.4. Quantitative evaluation

Three comparative evaluations are presented in this section that justify the selection of the adopted variant of the proposed approach and compare it against the state of the art. In all experiments, image $\nu = 14$th (700 nm) was selected as the reference and, thus, error for I_{14} is zero. In comparative evaluations of local methods, the same correspondences were utilized as input. Features due to markers were excluded from the homography estimation, so as not to provide additional information due to the markers. Besides figure plots corresponding to individual experiments, the results are also reported in aggregation in Tables 1 and 2.

First, affine and projective homographies were compared (Section 2.2). The results are plotted in Fig. 4. Affine homography provides less error and more robustness, even in D5 where camera and painting were not perpendicularly oriented. This is attributed to the mild surface inclination and fewer DOFs which reduce sensitivity to local minima in the optimization. The adopted variant is the affine (homest6), henceforth called *homest*.

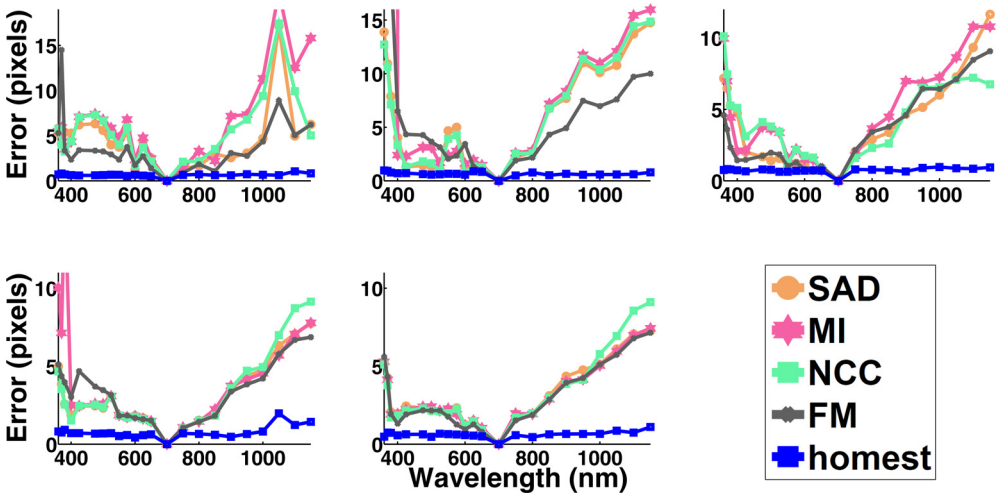

Fig. 6. Errors for the global matching methods versus homest registration, as a function of wavelength, for D1–D5 (left to right, top to bottom).

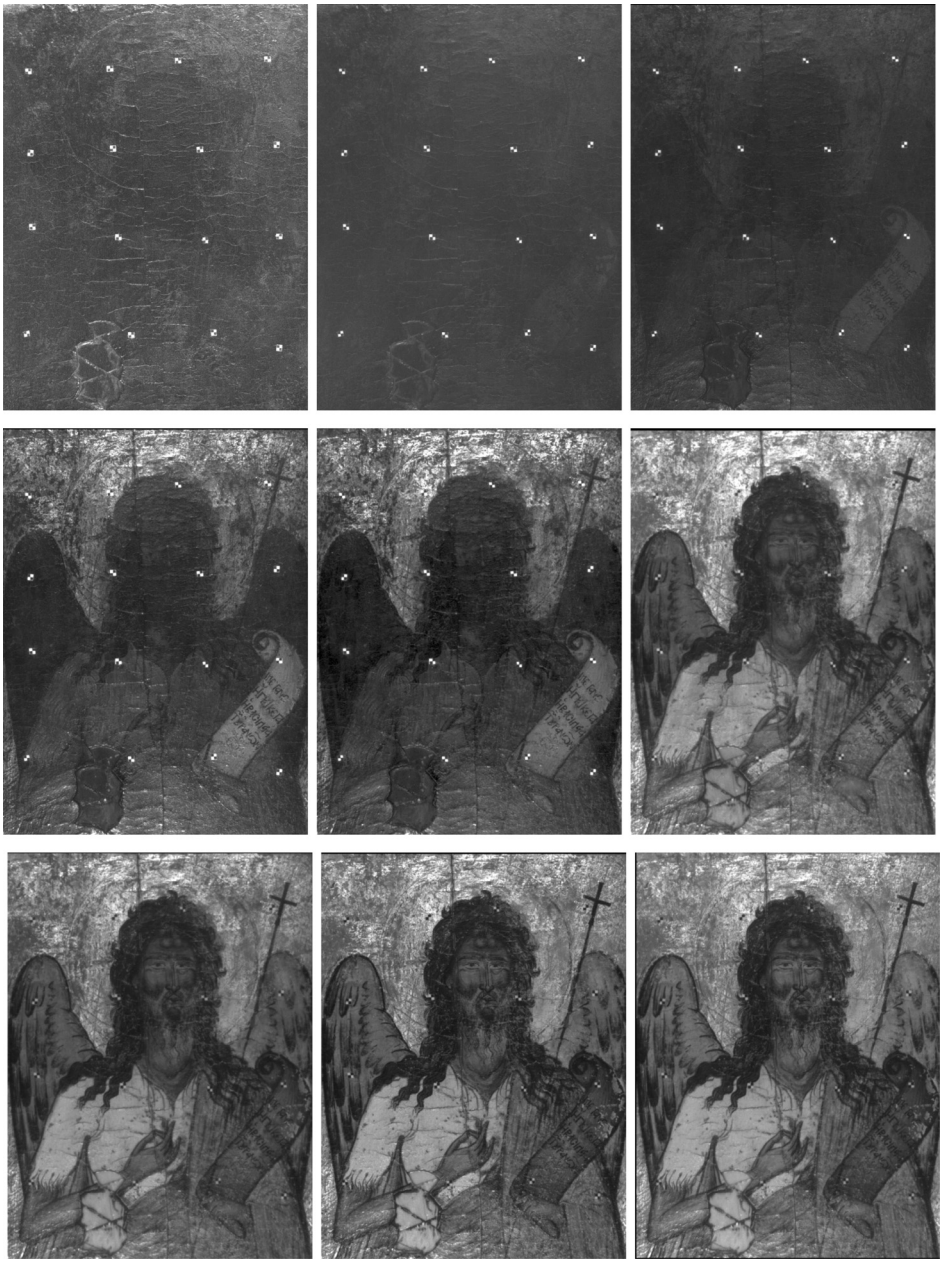

Fig. 7. Registration results for D2, using the homest method. Shown are S_i at 360, 380, 425, 500, 525, 750, 900, 1000, 1100 nm (top to bottom, left to right).

Second, accuracy of homest was compared against two state of the art local methods. The first was RANSAC [19] estimation for homography, followed by a robust least-squares fit of the homography to the inliers of the consensus and achieved by application of the Levenberg–Marquardt algorithm [28]. This method is henceforth referred as *RANSAC*. Second, *LMedS* refers to the same operation but, now, inliers are determined by the median reprojection error. As in RANSAC, the final result is computed by the same least-squares fit process, this time applied to the LMedS inliers. Results are shown in Fig. 5. All tested methods perform decently, however homest clearly outperforms the others. Unfortunately, we could not directly compare with the results in [21] as, in that work, evaluation elaborates on the mosaicing of images rather than registration between spectral bands. Moreover, no refocusing per spectral band is reported. Furthermore, a qualitative difference of the data in [21] is that the spectrum is very densely sampled (260 bands vs 23 in this work) and, thus, matching is facilitated because images are more similar. Both methods yield subpixel accuracy results, for images of similar resolution. The proposed work is faster by, approximately, an order of magnitude, due to the direct matching of keypoints.

Third, homest was tested against global methods. Homographies were globally estimated optimizing the Sum of Absolute Differences (SAD), Mutual Information (MI), and Normalized Cross Correlation (NCC), as the image difference objective functions. The following methods for unconstrained multivariable optimization were then tested for the optimization task: simplex search [33], Steepest Gradient Descent [34], Limited-memory BFGS [35] and BFGS Quasi-Newton [36]. The latter exhibited the best performance in preliminary tests and was selected. Moreover, the Fourier–Mellin (FM) global method [37] was also evaluated. In Fig. 6, registration errors for the global methods are plotted. In some cases, MI exhibits

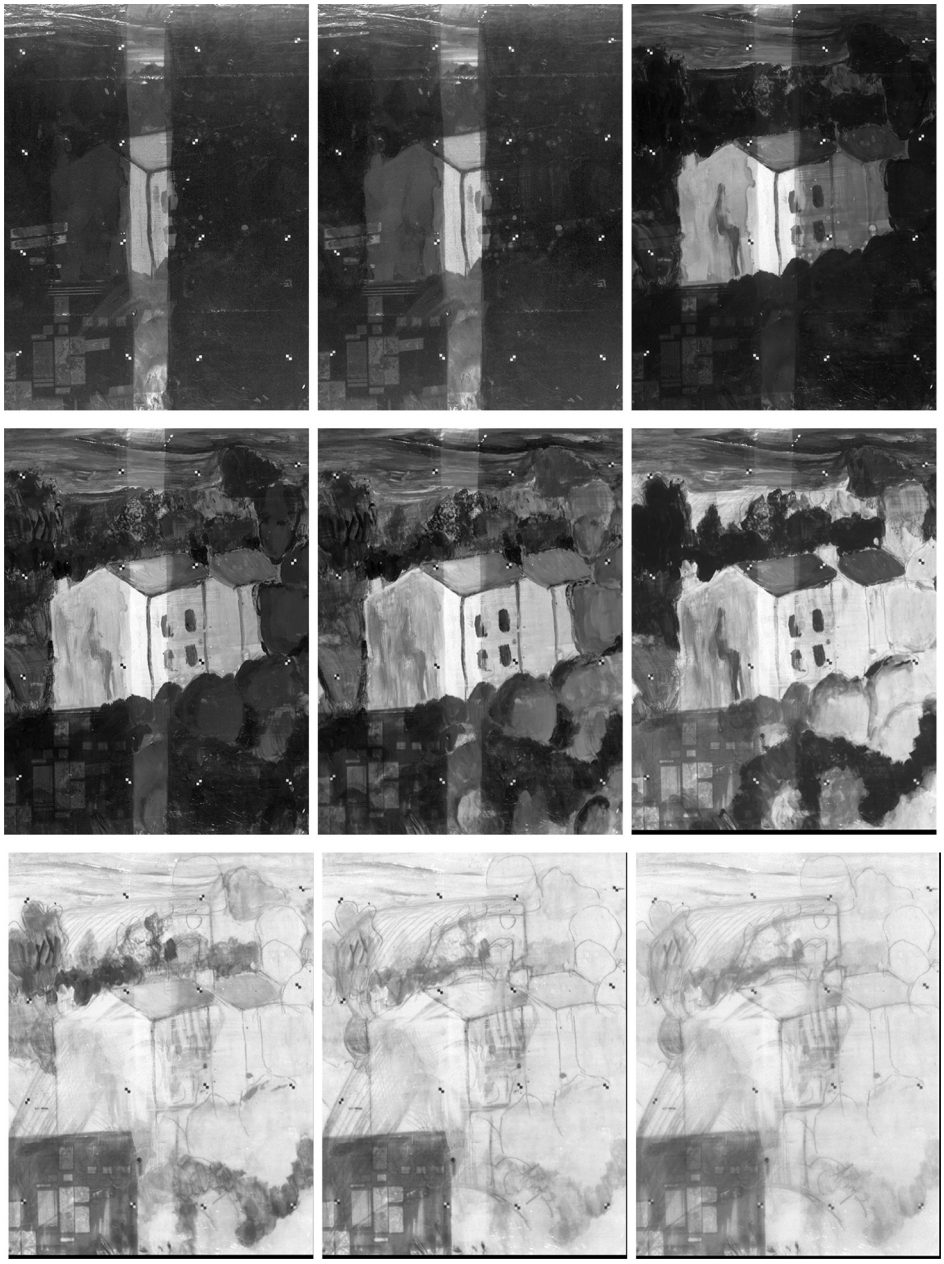

Fig. 8. Registration results for D5 using the homest method. Shown are S_i at 360, 380, 425, 500, 525, 750, 900, 1000, 1100 nm (top to bottom, left to right).

error greater than 1000 pixels and it is regarded as failed; this is noted as 'NA' in Tables 1 and 2. Also, very high error values are truncated in the plots of Fig. 6.

In Tables 1 and 2, the results of the aforementioned experiments are reported. Mean errors (and std) are reported in pixels and mm, respectively in the two tables. E_0 is particularly high for scenarios using the portable setup (D3–D5).

Registration results, for indicative images of D2 and D5 are shown in Figs. 7 and 8, respectively.

4. Conclusions

A MSI registration method for paintings is proposed. The method is based on keypoint matches across pairs of consecutive images, to estimate homographies that align these pairs. By linking these homographies, images of the MSI sequence are registered to a reference image, providing an aligned spectral cube. To comparatively and quantitatively evaluate the suggested or other MSI registration methods, a marker-based approach is proposed and benchmark datasets are publicly availed.

Experimental evaluation shows that, in the studied domain, global methods are less accurate than local. Inferior performance of global approaches, is attributed to content variation between wavelengths. Contrary, keypoints are less sensitive to such variations. Moreover, it is found that the homest homography estimation method outperforms the, widely employed, local registration methods based on RANSAC or LMedS. The algorithmic outcome is tested in *in-situ* scenarios, yielding subpixel accuracy and is found suitable for creating accurate spectral cubes with static or portable MSI systems.

Future work regards the implementation of similar experiments on more types of planar surfaces related to cultural heritage. Our intention is to investigate the applicability of the proposed approach in a broader range of materials encountered in cultural heritage objects and improve it as this extension of scope

may require. Another future goal is the update of the registration approach to minimize error for all pairs simultaneously, as in bundle adjustment [38], rather than individual pairs.

Acknowledgments

This work was supported by the Foundation for Research and Technology—Hellas, Institute of Computer Science (FORTH—ICS) internal RTD Programme "Ambient Intelligence and Smart Environments". This work was partly conducted in the framework of the POLITEIA research project, Action KRIPIS, project No. MIS-448300 (2013SE01380035) funded by the General Secretariat for Research and Technology, Ministry of Education, Greece and the European Regional Development Fund (Sectoral Operational Programme: Competitiveness and Entrepreneurship, NSRF 2007-2013)/European Commission. Authors thank Manolis I.A. Lourakis for help with application of [25].

References

[1] H. Liang, Advances in multispectral and hyperspectral imaging for archaeology and art conservation, Appl. Phys. A 106 (2) (2011) 309–323.
[2] C. Fischer, I. Kakoulli, Multispectral and hyperspectral imaging technologies in conservation: current research and potential applications, Stud. Conserv. 51 (1) (2006) 3–16.
[3] K. Melessanaki, V. Papadakis, C. Balas, D. Anglos, Laser induced breakdown spectroscopy and hyper-spectral imaging analysis of pigments on an illuminated manuscript, Spectrochim. Acta 56 (2001) 2337–2346.
[4] S. Kogou, A. Lucian, S. Bellesia, L. Burgio, K. Bailey, C. Brooks, H. Liang, A holistic multimodal approach to the non-invasive analysis of watercolour paintings, Appl. Phys. A 121 (3) (2015) 999–1014.
[5] V. Papadakis, Y. Orphanos, S. Kogou, K. Melessanaki, P. Pouli, C. Fotakis, Iris: a novel spectral imaging system for the analysis of cultural heritage objects, in: SPIE, vol. 8084, 2011, pp. 80840W-L 80840W-6.
[6] J. Delaney, J. Zeibel, M. Thoury, R. Littleton, M. Palmer, K. Morales, R. De La Rie, A. Hoenigswald, Visible and infrared imaging spectroscopy of Picasso's harlequin musician: mapping and identification of artist materials in situ, Appl. Spectrosc. 64 (6) (2010) 584–594.
[7] A. Cosentino, Panoramic, macro and micro multispectral imaging: an affordable system for mapping pigments on artworks, J. Conserv. Museum Stud. (2015) 1–17.
[8] J. Brauers, N. Schulte, T. Aach, Multispectral filter-wheel cameras: geometric distortion model and compensation algorithms, IEEE Trans. Image Process. 17 (12) (2008) 2368–2380.
[9] B. Zitova, J. Flusser, Image registration methods: a survey, Image Vis. Comput. 21 (2003) 977–1000.
[10] H. Liang, D. Saunders, J. Cupitt, A new multispectral imaging system for examining paintings, J. Imaging Sci. Technol. 49 (6) (2005) 551–562.
[11] H. Liang, A. Lucian, R. Lange, C.S. Cheung, B. Su, Remote spectral imaging with simultaneous extraction of 3D topography for historical wall paintings, ISPRS J. Photogramm. Remote Sens. 95 (2014) 13–22.
[12] J. Cupitt, K. Martinez, VIPS: an image processing system for large images, in: SPIE Conference on Imaging Science and Technology, vol. 1663, 1996, pp. 19–28.
[13] J. Brauers, T. Aach, Multispectral filter-wheel cameras: geometric distortion model and compensation algorithms, Image Anal. 5575 (2009) 119–127.
[14] G. Bianco, F. Bruno, M. Muzzupappa, Multispectral data cube acquisition of aligned images for document analysis by means of a filter-wheel camera provided with focus control, J. Cult. Herit. 14 (2013) 190–200.
[15] M. Lettner, M. Diem, R. Sablatnig, P. Kammerer, H. Miklas, Registration of multi-spectral manuscript images as prerequisite for computer aided script description, in: Computer Vision Winter Workshop, 2007, pp. 51–58.
[16] M. Diem, M. Lettner, R. Sablatnig, Multi-spectral image acquisition and registration of ancient manuscripts, in: AAPR/OAGM Workshop, vol. 224, 2007, pp. 129–136.
[17] M. Lettner, M. Diem, R. Sablatnig, H. Miklas, Registration and enhancing of multispectral manuscript images, in: European Signal Processing Conference, 2008, pp. 1–5.
[18] A. Cosentino, Identification of pigments by multispectral imaging: a flowchart method, Herit. Sci. 2 (8) (2014) 1–12.
[19] M. Fischler, R. Bolles, Random sample consensus: a paradigm for model fitting with applications to image analysis and automated cartography, Commun. ACM 24 (6) (1981) 381–395.
[20] D.M. Conover, J.K. Delaney, P. Ricciardi, M.H. Loew, Towards automatic registration of technical images of works of art, IS&T SPIE Electron. Imaging 7869 (2011).
[21] D. Conover, J. Delaney, M. Loew, Automatic registration and mosaicking of technical images of old master paintings, Appl. Phys. A 119 (4) (2015) 1567–1575.
[22] D. Lowe, Distinctive image features from scale-invariant keypoints, Int. J. Comput. Vis. 60 (2) (2004) 91–110.
[23] P. Fua, A parallel stereo algorithm that produces dense depth maps and preserves image features, Mach. Vis. Appl. 6 (1) (1993) 35–49.
[24] A. Vedaldi, B. Fulkerson, VLFeat: An Open and Portable Library of Computer Vision Algorithms, 2008 http://http://www.vlfeat.org/ (accessed 31.0116).
[25] M. Lourakis, homest: A C/C++ Library for Robust, Non-Linear Homography Estimation, 2006, Jul. http://www.ics.forth.gr/ourakis/homest/ (accessed 17.01.17).
[26] R. Hartley, In defense of the eight-point algorithm, IEEE Trans. Pattern Anal. Mach. Intell. 19 (6) (1997) 580–593.
[27] P. Rousseeuw, Least median of squares regression, J. Am. Stat. Assoc. 79 (388) (1984) 871–880.
[28] J. Nocedal, S. Wright, Numerical Optimization, Springer, 2006.
[29] M. Lourakis, levmar: Levenberg–Marquardt Nonlinear Least Squares Algorithms in C/C++, 2004, Jul. http://www.ics.forth.gr/lourakis/levmar/ (accessed 30.01.16).
[30] P. Karamaounas, A. Zacharopoulos, K. Hatzigiannakis, M. Andrianakis, K. Melessanaki, X. Zabulis, Multispectral image registration based on keypoint matching and homography estimation for cultural heritage artifacts. Technical Report TR-464, Institute of Computer Science (ICS), Foundation for Research and Technology – Hellas (FORTH), 2016, May.
[31] L. Dagum, R. Menon, OpenMP: an industry-standard API for shared-memory programming, IEEE Comput. Sci. Eng. 5 (1) (1998) 46–55.
[32] A. Geiger, F. Moosmann, O. Car, B. Schuster, Automatic calibration of range and camera sensors using a single shot, in: International Conference on Robotics and Automation, 2012.
[33] J.C. Lagarias, J.A. Reeds, M.H. Wright, P.E. Wright, Convergence properties of the Nelder–Mead simplex method in low dimensions, SIAM J. Optim. 9 (1) (1998) 112–147.
[34] M. Hestenes, E. Stiefel, Methods of conjugate gradients for solving linear systems, J. Res. Natl. Bureau Stand. 49 (1952) 409–436.
[35] R. Malouf, A comparison of algorithms for maximum entropy parameter estimation, in: Conference on Natural Language Learning, vol. 20, 2002, pp. 1–7.
[36] R. Fletcher, A new approach to variable metric algorithms, Comput. J. 13 (3) (1970) 317–322.
[37] B. Reddy, B. Chatterji, An FFT-based technique for translation, rotation and scale-invariant image registration, IEEE Trans. Image Process. 5 (8) (1996) 1266–1271.
[38] B. Triggs, P. McLauchlan, R. Hartley, A. Fitzgibbon, Bundle adjustment – a modern synthesis, in: International Conference on Computer Vision Workshops, 2000, pp. 298–372.